WORLD CONFERENCE ON TIMBER ENGINEERING 2025
BRISBANE, AUSTRALIA
Advancing Timber for the Future Built Environment

# EXPERIMENT ON AXIAL CAPACTY-BENDING CAPACITY RELATIONSHIP OF PLASITC HINGE OF STEEL BAR-TIMBER COMPOSITE COLUMN

Rin Kamimakise[1] , Keisuke Hayata[2] , and Shinichi Shioya[3]

**ABSTRACT:** In light of the current climate crisis, there has been much recent interest in using timber structural members in large buildings, since timber is as renewable natural resource, and moreover, in severe earthquake prone, such as Japan, they are more desired on the grounds of light weight of timber members. We are developing a frame system formed by timber members reinforced by deformed steel bars (i.e. rebars) using epoxy resin adhesive. We have already a technique for the connection between column of ground floor and reinforced concrete foundation. However, behavior of the column subjected to bending under higher axial force has been not investigated yet. In previous WCTE 2023, we reported bending characteristic of the other portion except hinge of the column derived from loading test and a calculation method for the bending moment capacity [1]. We have planned an experiment to investigate bending characteristic of the hinge of the column under bending and higher axial force. This paper reports the experiment, its results, and comparison of the experiment result and calculation on bending moment capacity.

**KEYWORDS:** *Composite timber, Column, Deformed steel bar, Moment capacity, Bending characteristic*

## 1 – INTRODUCTION

S.Shioya has proposed a structural system for building construction, adopting Hybrid Glulam Timber members using Steel bars (HGTSB, nicknamed "Samurai" in Japan) and has developed the structural design methodology [1]. Our team is now developing more refined and more competitive and commercial structural system for buildings adopting HGTSB and its structural design methodology.

## 2－BACKGROUND AND TARGET

S.Shioya has already developed a technique for rigid connection of rebars inside the composite timber, using carbon fiber plastic sleeve (CFS) and epoxy resin adhesive with works similarly to work process of the glued-in-rod, and reported performance of the column adopted the technique [1]. And then his group testified the application of the technique to the connection between column of ground floor and reinforced concrete (RC)foundation, by loading test of column specimens [1,2,3]. The connection is found to produce high bending capacity and abundant-energy dissipation up to large deformation. However, behavior of the column subjected to bending under higher axial force has been not investigated yet. In previous WCTE 2023, we reported bending characteristic of the other portion except hinge of the column derived from loading test and a calculation method for the bending moment capacity [4]. As shown in Figure 1, We have planned an experiment to investigate bending characteristic of the hinge of the column under bending and higher axial force. The column's bottom is assumed to be connected to RC foundation.

## 3 –COMPREESION TEST

At first, we conducted uniaxial compression loading test of the short column for the hinge portion of a column.

### 3.1 SPECIMEN AND LOADING

There were two types of test specimen: Glulam timber specimen (WO) and Composite specimen (HW). Figure 2(a) and (b) show the cross-section and dimensions of the specimens. The scale of the cross-section is 1/4 specimen.

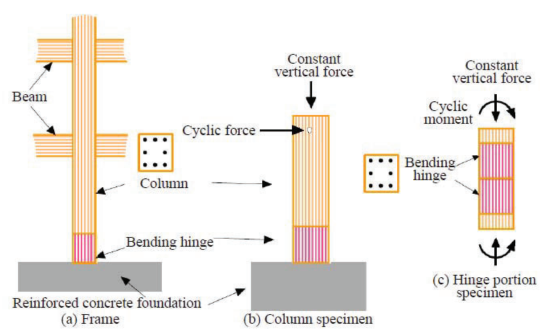


***Figure 1:*** *Column in frame, column specimen, and hinge*

[1] Rin Kamimakise, Department of Architecture, Kagoshima University, Kagoshima, Japan, k6194691@kadai.jp

[2] Toshihisa Ishii, Department of Architecture, Kagoshima University, Kagoshima, Japan, k3431122@kadai.jp

[3] Shinichi Shioya, Department of Architecture, Kagoshima University, Kagoshima, Japan, k7347039@kadai.jp


https://doi.org/10.52202/080513-0690

The number of rebars in the HW specimen was eight. The ratio of rebar's gross area to the full cross-section ($B$ $D$) is 4.50%. The side of the specimen are shown in Figure 2(c) and (d). There are five WO specimens and four HW specimens.
The species of the Glulam timber was Japanese cedar, and the lamina did not have finger joints. The grade of the laminas was the same as that used for Grade L70, which is E65-F255. Table 1 shows the mechanical properties of

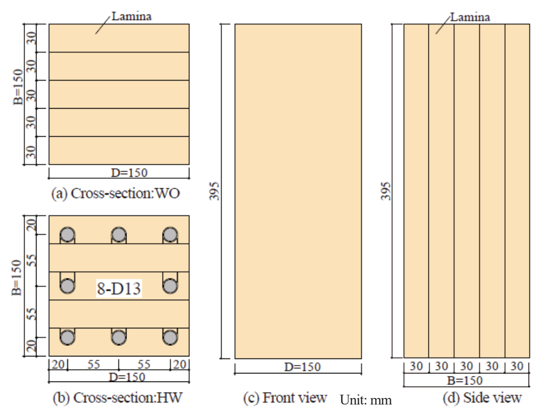


***Figure 2:*** *Cross-section and side view of specimen*

***Table 1:*** *Properties of lamina*

| Lamina | Compressive test | | Tensile test | | Bending test | |
|---|---|---|---|---|---|---|
| Grade | E | F | E | F | E | F |
| L70 | 8626 | 41.8 | 8258 | 49.0 | 8981 | 66.0 |

The number of testpieces at each test: 5, E:Young's modulus, F:Strength

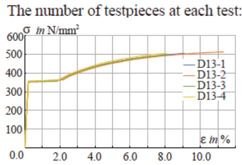


***Figure 3:*** *Stress-strain curve of rebar under tensile*

***Table 2:*** *Properties of rebar*

| Rebar | E | $\sigma_y$ | $\sigma_u$ |
|---|---|---|---|
| D13 | $1.84 \times 10^5$ | 351 | 530 |

E: Young's modulus, $\sigma_y$: Yield strength
$\sigma_u$: Tensile strength Unit: N/mm$^2$

the laminas. Compression, tension and bending tests were conducted on the laminas. The average moisture content of the laminas was 12.8% for the six test pieces. Table 2 shows the mechanical properties of the rebars as determined by material testing. The rebars were D13 with SD345 material. Figure 4 shows the tensile stress-strain relationship for the rebars. Strain hardening is clear in the stress-strain relationship of mild steel from around 2%. Manufacturing of the specimens, loading and measurement were the same in Reference 2. Please refer to those.

## 3.2 EXPERIMENTAL RESULTS

Table 3 lists specimens, their dimensions, and experimental values. The stress-strain relationship is shown in Figure 4. The vertical axis is the value obtained by dividing the compression load by the cross-sectional area ($B$ $D$) of the specimen, and the horizontal axis is the value obtained by dividing the average compressive deformation by the height (h) of the specimen.

### (a) Glulam timber specimen WO

Figure 4(a) shows the stress-strain relationship for WO. The relationships for all five specimens were similar. the compressive strength was maintained until approximately 1.25%, after which the compressive stress gradually decreased as the strain increased. There was some variation in the range of decreasing stress.

### (b) Steel bar-timber composite specimen HW

Figure 4(b) shows the relationship of the HW compared to the WO-2. HW specimens have increased elastic stiffness and compressive strength compared to the WO-2, and the strain at which the compressive strength can be maintained (hereafter, the limit strain) also increased. The compressive strength

***Table 3:*** *Specimens and experiments*

| Specimen | $B$ | $D$ | $h$ | Rebar | $p_g$ | ${}_eF_m$ | ${}_e\sigma_m$ | ${}_e\sigma_{m\text{-}ave}$ | ${}_cF_m$ | ${}_c\sigma_m$ | ${}_eF_y$ | ${}_eF_{y\text{-}ave}$ | $\varepsilon_p$ | $\varepsilon_m$ | $\varepsilon_{90}$ | $\varepsilon_f$ | E | $E_{ave}$ | Failure |
|---|---|---|---|---|---|---|---|---|---|---|---|---|---|---|---|---|---|---|---|
| | mm | mm | mm | | % | kN | N/mm$^2$ | N/mm$^3$ | kN | N/mm$^2$ | kN | kN | $\times 10^{-6}$ | $\times 10^{-6}$ | $\times 10^{-6}$ | $\times 10^{-6}$ | N/mm$^2$ | N/mm$^2$ | |
| WO-1 | 150.1 | 150.1 | 395.9 | - | 0.00 | 682 | 30.2 | | | | 471 | | 3545 | 8279 | 14266 | 17723 | 6008 | | Wood crush |
| WO-2 | 150.3 | 150.2 | 395.9 | - | 0.00 | 707 | 31.3 | | | | 463 | | 3598 | 9386 | 18715 | 25809 | 5783 | | Wood crush |
| WO-3 | 150.4 | 150.1 | 395.6 | - | 0.00 | 712 | 31.5 | 31.2 | 705 | 31.2 | 428 | 440 | 3404 | 9689 | 15714 | 26555 | 5565 | 5818 | Wood crush |
| WO-4 | 150.2 | 150.2 | 396.6 | - | 0.00 | 705 | 31.2 | | | | 409 | | 3316 | 12059 | 18339 | 28851 | 5520 | | Wood crush |
| WO-5 | 150.2 | 150.1 | 397.5 | - | 0.00 | 719 | 31.9 | | | | 429 | | 3088 | 10185 | 14327 | 34812 | 6213 | | Wood crush |
| HW-1 | 150.4 | 150.5 | 395.7 | 8-D13 | 4.48 | 1043 | 46.1 | | | | 703 | | 2441 | 19022 | 24003 | 26808 | 13265 | | Rebar buckling |
| HW-2 | 150.3 | 150.8 | 392.2 | 8-D13 | 4.47 | 1060 | 46.7 | 46.9 | 1031 | 45.6 | 723 | 706 | 2317 | 16113 | 21772 | 21772 | 13899 | 13566 | Rebar buckling |
| HW-3 | 150.3 | 150.3 | 396.2 | 8-D13 | 4.49 | 1085 | 48.1 | | | | 721 | | 2357 | 15070 | 24149 | 24149 | 13604 | | Rebar buckling |
| HW-4 | 150.2 | 150.5 | 395.9 | 8-D13 | 4.48 | 1056 | 46.7 | | | | 677 | | 2271 | 12958 | 21966 | 21966 | 13497 | | Rebar buckling |

*B, D, h*: Width, depth, and height of column, $p_g$: Rebar ratio to the gross area of column, ${}_eF_m$: Axial force capacity, ${}_eF_{m\text{-}ave}$: Average of ${}_eF_m$, ${}_e\sigma_m$: Stress of ${}_eF_m$, ${}_e\sigma_{m\text{-}ave}$ : Average of ${}_e\sigma_m$, ${}_cF_m$ : Value calculated for ${}_eF_m$, ${}_c\sigma_m$: Value calculated for ${}_e\sigma_c$, $\varepsilon_p$: Axial strain at propotional limit by displacement, $\varepsilon_m$: Axial strain at maximun capacity, $\varepsilon_{90}$ : Axial strain at 90% of maximun capacity after peak by displacement, $\varepsilon_f$ : Axial strain at the final loading by displacement, E: Young's modulus, $E_{ave}$: Average of E, Failure: Failure mode determining ductility

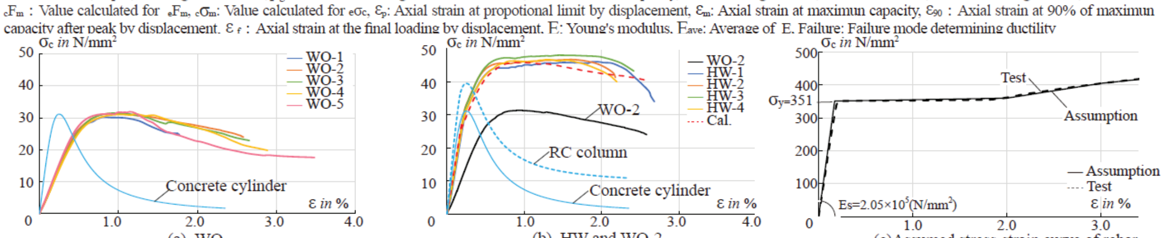


***Figure 4:*** *Compressive stress-strain curves*

https://doi.org/10.52202/080513-0690

increased to about 1.60 times the average value of WO, and it was maintained up to a compressive strain of 2.0%.

For curve calculated shown in Figure 4(b), the stress-strain relationship of timber is assumed to be as the WO-2 relationship, and the stress-strain relationship of rebar is assumed to be a trilinear relationship with a solid line in Figure 4(c). Young's modulus Es of rebar was assumed to be the standard value of $2.05 \times 10^5$ N/mm$^2$.

By the calculation curve, the initial stiffness is estimated from the calculated stress-strain relationship, and the proportional limit strength and compressive strength is also estimated.

### 3.4 COMPARISION WITH REINFORCED CONCRETE COLUMN

Figure 4(a) shows the relationship calculated by assuming that the compressive strength of concrete is the average compressive strength of WO, 31.2 N/mm$^2$, and the compressive strain at the strength is 0.25%, shown by light blue solid line. The relationship for concrete used Popovics' curve. Young's modulus of timber is significantly smaller than that of concrete, but the strain at which the compressive strength can be maintained is greater in timber after about 0.5%.

In RC columns, the upper limit of the rebar ratio pt of the tensile rebar is limited to 1.0% in order to prevent bond failure of rebar and ensure ductility. On the other hand, as no bending cracks occur in timber of the composite member before rebars yield, the adhesion stress is reduced, and adhesion failure hardly occurs. So the $p_t$ can be set to large. The $p_g$ of HW is 4.50%. Figure 4(b) shows the compressive stress-strain relationship of RC columns calculated by replacing the timber in HW with concrete, using the light blue dotted curve. The $p_g$ of the RC column was calculated as 2.64% (=0.588 x 4.50). The relationship of concrete was assumed to be that of the light blue by Popovic equation in Figure 4(a), and the relationship of rebar was assumed to be that of Figure 4(c). The elastic stiffness of the HW of the composite timber column approaches the initial stiffness of the RC column as the amount of rebar increases, and the compressive strength becomes 1.16 times that of the RC column, and the ductility also becomes extremely large. The composite column, if the cross-sectional dimensions ($B$ $D$) are the same, demonstrates extremely superior compressive properties compared to the RC column, except for compressive stiffness.

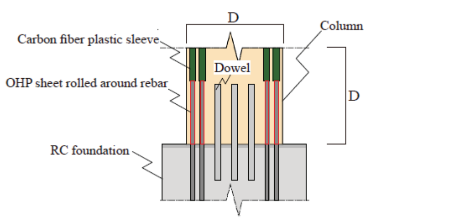


*Figure 5: Connection of Column's base and RC foundation*

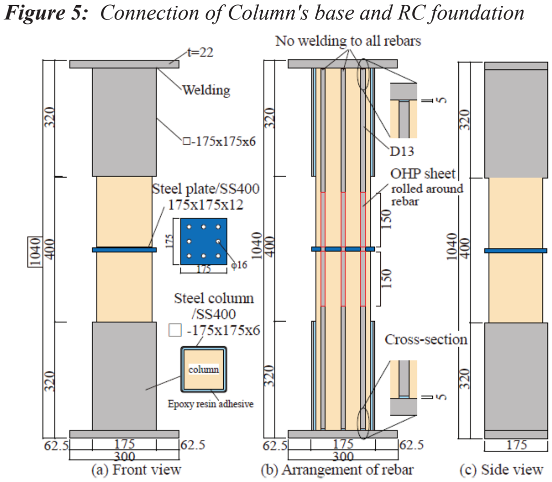


*Figure 6: Specimen for bending*

*Table 4: Specimen and target of axial force*

| Specimen | $\eta_w$ | $\eta$ | $N$ in kN |
|---|---|---|---|
| HW(NM05) | 0.05 | 0.03 | 35.2 |
| HW(NM20) | 0.20 | 0.13 | 141.0 |
| HW(NM40) | 0.40 | 0.27 | 282.0 |
| HW(NM60) | 0.60 | 0.40 | 423.0 |
| HW(NM80) | 0.80 | 0.53 | 564.0 |
| HW(NM110) | 1.10 | 0.73 | 775.4 |
| HW(NM130) | 1.30 | 0.86 | 916.4 |

$\eta_w = N/N_{max\text{-}w}$, $\eta = N/N_{max}$, $N$: Axial force

$N_{max\text{-}w}$: Average of axial capacitis of WO specimen by compressive test,i.e.705kN

$N_{max}$: Average of axial capacitis of HW specimen by compressive test,i.e.1061kN

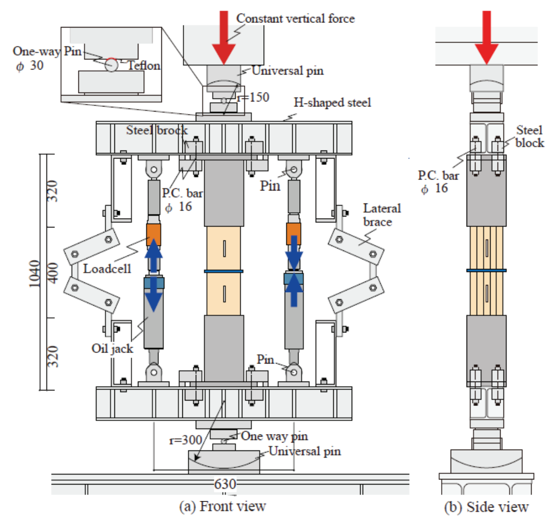


*Figure 7: Setup for loading*

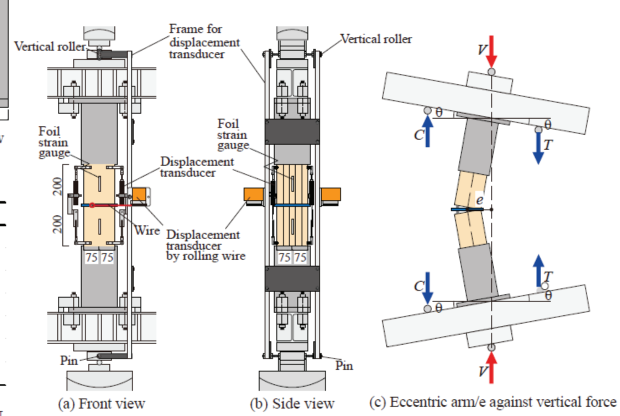


*Figure 8: Setup for measurement of displacement and deformations*


https://doi.org/10.52202/080513-0690

## 4 − REPEATIVE BENDING LAODING TO COLUMN UNDER VERTICAL LOAD

### 4.1 SPECIMEN

As shown in Figure 5, the column is joined to RC foundation at the ground story. As timber cannot resist tensile force at the joint surface, it is assumed that it will only resist compressive axial force and bending compressive force, and that shear force will be transmitted by round steel dowels, and that the rebar will resist the tensile and compressive forces. When the rebar yields in tension, sprit cracks will appear in the wood around the rebar, so previous studies have devised a way to prevent the cracks [2,3]. In the device, the length of the yield section of rebar is limited to the length of D, and in other sections, the rebar and timber resist as one so that the assumption of plane section retention is satisfied [2,3].

In this experiment, in order to facilitate the application of axial force and moment, the shape of the test specimen was made symmetrical vertically, as shown in Figure 6(a), and a stub made of square steel pipe was provided to secure the anchorage of the rebars. The test section was between the upper and lower steel pipes, and a steel plate (hereafter, divided steel plate) was inserted at the center height to create a form in which the yield hinge parts exist above and below the divided steel plate. In the case of compression failure of wood, failure progresses in the direction with more weak points in the upper and lower hinge portions. The portion with no progress of failure means that the performance is higher than that with progress of failure. The cross-section of specimen is the same as that of the specimen in Figure 2. The column was subjected to bending stress in the direction of the weak axis. The upper and lower parts were inserted into square steel pipes and filled with epoxy adhesive to join them. The timber column was divided into two parts at the top and bottom, and a split steel plate was inserted between them to fix the upper and lower timber, and the column was made by filling the holes for the steel bars with the specified amount of epoxy adhesive and inserting the steel bars into the holes and bonding them. The split steel plates had 8-holes with a diameter of 16 mm in the positions of the rebars.

As shown in Figure 6(b), all the rebars are continuous from the end plate of the lower steel pipe to the end plate of the upper steel pipe. However, as shown in the details of the rebars and end plates in Figure 6(b), there is a 5 mm gap, which is filled with epoxy adhesive. On the top and bottom of the split steel plate, OHP film (thickness: 0.1mm) are bonded to the inside of the holes in the steel bars using epoxy adhesive over a length of 150mm. The rebars pass through a hole rolled by the film and the epoxy adhesive fills the space between the rebar and the OHP film. This effect has been reported in previous studies [2,3].

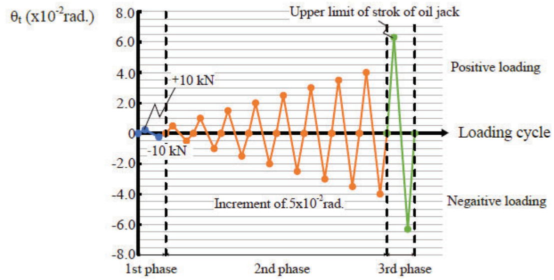


***Figure 9:*** *Protocol for loading by bending*

To prevent the steel plates from adhering to the timber, an oil-based paint was applied to the entire surface of the steel plates to form a coating. Table 4 shows a list of the test specimens, the axial force ratio, and the axial force. The axial force ratio $\eta_W$ was defined as the ratio of the constant vertical load applied to the maximum load (experimental value) of WO in the uniaxial compression test (705 kN). There was one type of specimens, which was the composite column HW, and there were seven specimens. The variable of the specimen was the axial force ratio, and the specimens were named as NM axial force ratio. The axial force ratio was the value of $\eta_W$ in Table 4 expressed as a percentage. Properties of wood of the specimens was same as that of uniaxial compression test.

### 4.2 LOADING AND MEASUREMENT

Steup for loading is shown in Figure 7. After a constant vertical load was applied to the specimen by installing a bending loading device in the test section of a 2000 kN long column pressure testing machine, a moment was applied to the column.

The force was applied by loading the column with a vertical load using a pressure testing machine, and repeated bending force was applied. Figure 9 shows the protocol of loading (target rotation angle $\theta_t$) used as the target for force application. In the first cycle, the load was applied at ±10 kN, and thereafter the $\theta_t$ was gradually increased in increments of 0.5 x $10^{-2}$ rad. and positive and negative cyclic loads were applied. Figure 8 shows the positions where the strain gauges were attached and the measurement sections for deformation. Strain gauges (length: 60 mm) were attached to the surface of the timber. One was attached to each side of the upper and lower hinge sections.

The displacement transducers were attached to the steel plates screwed to the timber of locations close to the upper and lower steel pipes, and the vertical axial deformation was measured at four locations. The deformation measured in this way is the value that occurs in the two hinge sections at the top and bottom. The horizontal displacement of the divided steel plate relative to the upper and lower one-way pins was measured using two rolling-type displacement transducers (the red line in Figure 8(a) is the wire).

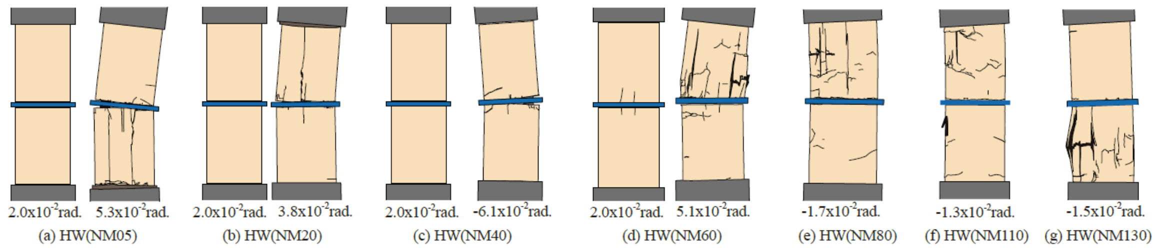


***Figure 10:*** *Final failures on front view*

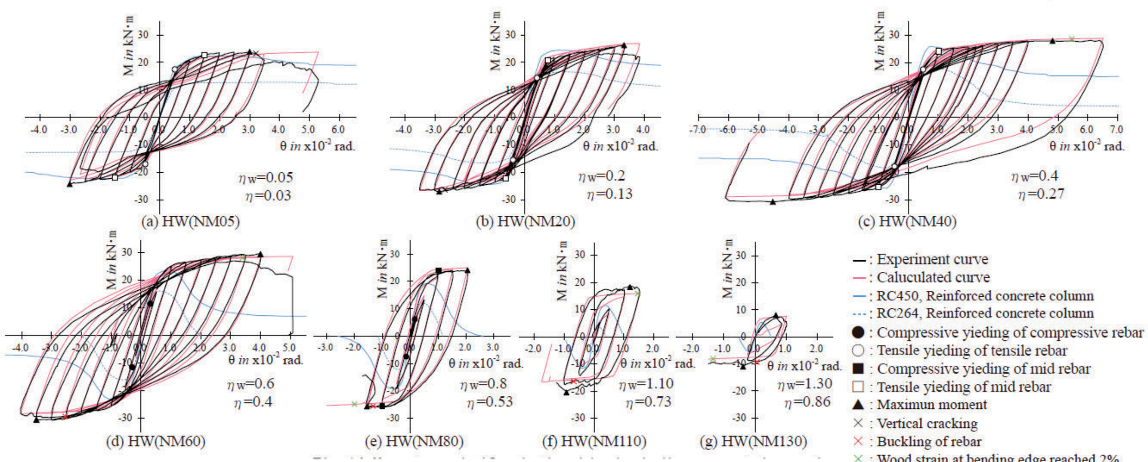


***Figure 11:*** *Moment-angle/θ relationship including eccentric arm/e*

### 4.3 BENDING MOMENT OF COLUMN

Figure 8(c) shows the deformation of the specimen when bending. When a moment is applied to the column, the cross-section at the center height of the column moves horizontally from its initial position. If the horizontal distance is defined as the eccentric distance $e$, the cross-section is also subjected to an additional moment of $V$ e due to the vertical load $V$. The maximum moment $M_u$ in the test section is expressed by Equation (1), and as the vertical load $V$ is increased, the additional moment also increases. The eccentric distance $e$ is the deformation measured by the displacement transducers.

$$Mu = C(\ell - e) + T(\ell + e) + Ve \qquad (1)$$

where, $C$ : Compressive force of the bending load oil jack, $T$ : Tension force of the bending load oil jack, $\ell$ : Horizontal distance from the upper and lower one-way pins to the bending load oil jack, $e$ : Horizontal distance of the cross-section of the center height of the test section to the line of action of the vertical load, $V$ : Vertical load

### 4.4 FAILURES

Figure 10 shows failures at $2.0\text{x}10^{-2}$ rad. and at the final stage. When $\eta_w$ was 0.05 to 0.6, the load could be applied up to a rotation angle greater than $2.0\text{x}10^{-2}$ rad., but when $\eta_w$ was 0.8 to 1.3, the load could only be applied up to the target rotation angle of $2.0\text{x}10^{-2}$ rad. or less.

For $\eta_w$ values between 0.05 and 0.4, as can be seen in Figure 10(a) to 10(d), there was almost no damage to the timber up to $2.0\text{x}10^{-2}$ rad. The composite timber columns have the characteristic of not being damaged even in major earthquakes.

At low axial forces of $\eta_w$ = 0.05 and 0.2, there was almost no damage up to $3.0\text{x}10^{-2}$ rad. and vertical cracks appeared on the column face at $3.5\text{x}10^{-2}$ rad. In cycles after this, the cracks expanded and the column was divided, and the bending capacity gradually decreased. However, the vertical load was supported. This is be a characteristic of columns in which the column foot bends and yields under low axial force.

Even when the applied force was increased to a large deformation angle of $+6.5\text{x}10^{-2}$ rad., there was almost no damage to the timber when $\eta_w$ was 0.4. When $\eta_w$ was between 0.05 and 0.4, there was no vertical crack or buckling of the main column bars.

At $\eta_w$ = 0.6, vertical cracks similar to those near the steel plates occurred in the timber up to $2.0\text{x}10^{-2}$rad. However, at $-4.0\text{x}10^{-2}$ rad. in the cycle, vertical cracks occurred in the timber due to buckling of the main bars on the compression side, and the bending capacity decreased rapidly, leading to failure.

For specimens with $\eta_w$ values between 0.8 and 1.3, the yield strength was reached in cycles of $2.0\text{x}10^{-2}$ rad. or less, and vertical cracks and buckling of the rebar occurred, resulting in a rapid decrease in yield strength and a situation where the vertical load could not be supported.

 https://doi.org/10.52202/080513-0690

### 4.5 MOMENT-ROTATION RELATIONSHIP

***Table 5:*** *Experimental results*

| Specimen | $\eta_w$ | $\eta$ | N | LD | EI | $M_y$ | $M_m$ | $\theta_u$ | $M_u$ | $M_u/M_m$ |
|---|---|---|---|---|---|---|---|---|---|---|
| HW(NM05) | 0.05 | 0.03 | 35.25 | + | 6.48 | 17.50 | 23.9 | 3.47 | 21.0 | 0.88 |
| | | | | - | -6.54 | -17.00 | -24.3 | -3.01 | -24.3 | 1.00 |
| HW(NM20) | 0.20 | 0.13 | 141 | + | 6.52 | 14.35 | 20.8 | 3.85 | 20.8 | 1.00 |
| | | | | - | -7.38 | -15.50 | -27.1 | -3.52 | -26.5 | 0.98 |
| HW(NM40) | 0.40 | 0.27 | 282 | + | 6.48 | 17.50 | 27.9 | 6.53 | 26.9 | 0.96 |
| | | | | - | -7.16 | -17.90 | -30.8 | -6.12 | -29.3 | 0.95 |
| HW(NM60) | 0.60 | 0.40 | 423 | + | 6.76 | 11.50 | 29.5 | 4.30 | 24.5 | 0.83 |
| | | | | - | -7.19 | -11.50 | -30.6 | -4.00 | -29.0 | 0.95 |
| HW(NM80) | 0.80 | 0.53 | 564 | + | 7.05 | 6.20 | 24.1 | 2.05 | 24.1 | 1.00 |
| | | | | - | -9.38 | -7.50 | -25.7 | -1.55 | -25.7 | 1.00 |
| HW(NM110) | 1.10 | 0.73 | 775.5 | + | – | – | 18.3 | 1.5 | 16 | 0.87 |
| | | | | - | | | -20.5 | -1.25 | -17.3 | 0.84 |
| HW(NM130) | 1.30 | 0.86 | 916.5 | + | – | – | 8.1 | 0.93 | 6.8 | 0.84 |
| | | | | - | | | -11.0 | -0.5 | -9.5 | 0.86 |

$\eta_w$: Ratio of axial force to average axial strength (705kN) of timber column specimen,
$\eta$: Ratio of axial force to average axial strength (1061kN) of steel bar-timber composite column specimen, *N*: Axial force *in* kN, LD: Loading direcrion,
*EI*: Bending stiffness *in* $\times 10^2$ kN·m$^2$, $M_y$: Yielding moment *in* kN·m,
$M_m$: Bending moment capacity *in* kN·m, $\theta_u$: Rotaional angle of column's hinge at ultimate moment when $M_m$ decreases rapidly. *in* $\times 10^{-2}$rad., $M_u$: Bending moment at $\theta_u$ *in* kN·m

The moment-angle relationship is shown in Figure 11. The moment was calculated using the value from Equation (1), and the angle was calculated as half the angle of rotation ($\theta$ in Figure11(c)) measured from the axial deformation of the column in the direction of the material axis using the displacement meter in the test section in Figure11. However, in the test piece with $\eta_w$= 1.3, when the target vertical load (916.4 kN) was applied, the compression resistance of the steel-framed timber in the uniaxial compression test was 86%, the lateral strain of the timber increased, the screws on the steel plate used to fix the displacement meter attached to the timber loosened, and the aforementioned rotation angle changed irregularly, so the rotation angle was calculated as the horizontal deformation of the divided steel plate, i.e. the eccentric distance e divided by the vertical distance (1528/2 mm) from the upper and lower one-way pins to the divided steel plate distance (1528/2mm) divided by the eccentric distance e. The pink loop and blue curve are the results of the calculations in Section 5.3 below.
When $\eta_w$ is 0.05-0.4, the stiffness decreases due to the separation of the timber and the split steel plate and the yielding of the tension rebar and the middle rebar, until the maximum capacity.
For the specimens with $\eta_w$ of 0.05 and 0.2, the point at which a vertical crack appeared on the column face is indicated by an ×. The maximum strength was determined by this crack. The strength was maintained stably up to $3.0 \times 10^{-2}$rad.
For the specimen with $\eta_w$ of 0.4, the strength was maintained stably up to $6.5 \times 10^{-2}$ rad.

For specimens with $\eta_w$ of 0.6 or more, the point at which vertical cracks occurred due to buckling of the main compression rebar is indicated by an X. For the specimen with $\eta_w$ of 0.6, the bending capacity remained stable up to the $+4.0 \times 10^{-2}$ rad. cycle, but cracks due to buckling of the main compression rebar occurred in the $-4.0 \times 10^{-2}$ rad. cycle, and the bending capacity decreased.
When $\eta_w$ was 1.1 or more, the load at which all the rebars yielded in the uniaxial compression test exceeded the load at which the specified vertical load was introduced, so the moment-rotation angle relationship does not show the point at which the rebars yielded in compression. The shape of the loop changed from a spindle shape to a bilinear shape of elasto-plasticity, which is different from the shape of the test piece with $\eta_w$ of 0.8 or less. In the case of specimens with $\eta_w$ of 1.1 or more, this shape is not particularly noticeable. As the axial force increases, even after the axial force is introduced, the entire surface maintains a state of compression even when bending force is applied, and there is no tensile region where only the rebar resists tension. This is thought to be because the characteristics of the compression side of the stress-strain relationship of the timber and rebar directly affect the moment-rotation angle relationship.

### 4.6 EXPERIMENTAL VALUES

Table 5 shows a list of experimental values for bending stiffness *EI*, yield moment $M_y$, bending capacity $M_m$, critical rotation angle $\theta_u$, and the moment at that time, for both positive and negative loads. The moment is the value according to Equation (1). The ratio $\eta$ of the vertical load *V* to the average axial capacity (1061 kN) of the uniaxial compression test specimen HW of the composite timber is also shown.
For specimens with a axial force ratio $\eta_w$ of 1.1 or more, *EI* and $M_y$ are not shown because the rebar yielded in compression when axial force was applied, exceeding the proportional limit. The critical rotation angle $\theta_u$ is defined as the rotation angle at the point where the moment decreases rapidly as the rotation angle increases due to the application of force after the bending capacity is reached and the moment decreases to 80% of $M_m$. However, as can be seen in Figure 11(a) and Figure 11(d) on the positive load side, if the specimen collapses due to repeated loading after reaching the bending strength and does not reach 80%, the maximum rotation angle of the previous cycle was taken as the critical rotation angle. The moment $M_u$ at the point when the critical rotation angle was identified for each test piece differs from the ratio $M_u$ / $M_m$ for the bending capacity $M_m$. This value is also shown on the far right of Table 5. Values of 0.9 or less are shown in light grey. The critical rotation angle was determined for all test pieces at a moment of approximately 83% or more of the bending capacity.

## 5 − ESTIMATION FOR BENDING CAPACITY

### 5.1 COMPATIBILITY OF GENERALIZED SUPPERPOSED STRENGTH TO THE COMPOSITE COLUMN

When the materials of a member have sufficient plastic deformation capacity, it has been demonstrated by the generalized superposed strength method and loading tests that the bending strength of the member can be estimated by dividing the cross-section into components and adding up the bending capacity of each component in such a way that the sum of the bending capacity of each component is maximized.
This bending strength is referred to as the strength based on the generalized superposed strength method based on

plasticity and is often applied to reinforced concrete and steel concrete columns. In the calculation of bending strength in RC columns, it is assumed that concrete resists only compression, but the compressive strain that can maintain compressive strength is around 0.3%, which does not have sufficient plastic deformation performance, so the compressive strength of concrete is reduced to compensate for that.

As shown in Figure 4(b), the compressive strength of the column made of wood can be maintained up to a compressive strain of 2.0%, and the value is about 7.0 times that of concrete, so it is expected that the accuracy of the estimation of bending strength using the generalized superposed strength method will be high.

## 5.2 CORRELATION CURVE BETWEEN AXIAL FORCE AND BENDING STREGTN CAPCITY

Figure 12 shows the resisting components of the column cross-section, divided into rebars and timber. The rebar is divided into tension rebar, intermediate rebar and compression rebar. The rebar is assumed to be rigid-plastic, and when it reaches its tensile or compressive yield strength, it is assumed to maintain its yield strength $\sigma_y$ for any further increase in strain. Figure12(a) shows the case where only tension and compression rebar are used, and the yield moment $M_{ry}$ when the axial force is zero is expressed by Equation (2). The yield capacity $N_{ry}$ when the bending moment is zero and only the compressive or tensile axial force is acting is expressed by Equation (3). The change in the moment $M_{ro}$ that can be resisted when the axial force $N$ changes between the tensile yield capacity and the compressive yield capacity (hereafter, the $N_{ro}$-$M_{ro}$ relationship) is expressed by Equation (4).

$$M_{ry} = a_t \sigma_y j \tag{2}$$
$$N_{ry} = 2\, a_t \sigma_y \tag{3}$$
$$M_{ro} = M_{ry}\,(1 - |N / N_{ry}|) \tag{4}$$

where, $a_t$: cross-sectional area of tensile rebar, $a_c$: cross-sectional area of compression rebar, which is assumed to be equal to $a_t$, $\sigma_y$ : yield strength of rebar, $j$: distance between centers of tensile and compression rebars, $N$: axial force

The $N_{ro}$-$M_{ro}$ relationship in Equation (4) is shown in Figure 13(a) as a black solid line. It is based on the dimensions of the column cross-section of the specimen, the yield strength (351 N/mm$^2$) of the rebar, and the compressive strength (31.2 N/mm$^2$) of the timber column. As the test is based on a column, the axial force is assumed to be positive for compression and negative for tension.

As shown in Figure12(b), the relationship between axial force $N$ and moment $M_{rm}$ ($N_{rm}$-$M_{rm}$ relationship) that can be resisted when the middle rebar is taken into account becomes the red polyline connecting points A, B, C and D in Figure13(a).

The black $N_{ro}$-$M_{ro}$ relationship polyline in Equation (4) becomes a red broken line in which the axial force is parallel-shifted by the amount of the yield strength of the middle rebar $a_m \sigma_y$ ($a_m$: cross-sectional area of the middle rebar) in the compression or tension direction.

Figure12(c) shows the resistance state of the timber, where it is assumed that it does not resist tension, but that it yields in compression with rigid plasticity, and that it can maintain its compressive strength $F_{wc}$ against further increases in strain. The change in the moment $M_w$ that can be resisted when the axial force $N$ changes from zero to the compressive strength $N_{wc}$ of the timber (hereafter, the $N_w$-$M_w$ relationship) is expressed by Equation (5).

$$M_w = 0.5\, N D\, \{ 1 - N / (F_{wc}\, b\, D) \} \tag{5}$$

where, $D$ : column depth, $b$ : column width

$F_{wc}$ : compressive strength of timber

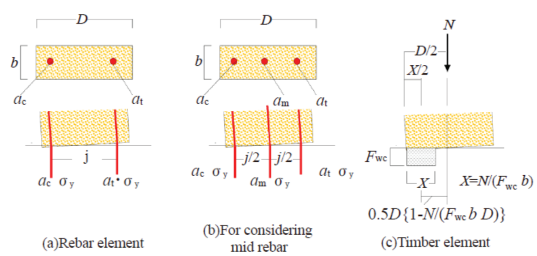


***Figure 12:** Elements against moment and axial force*

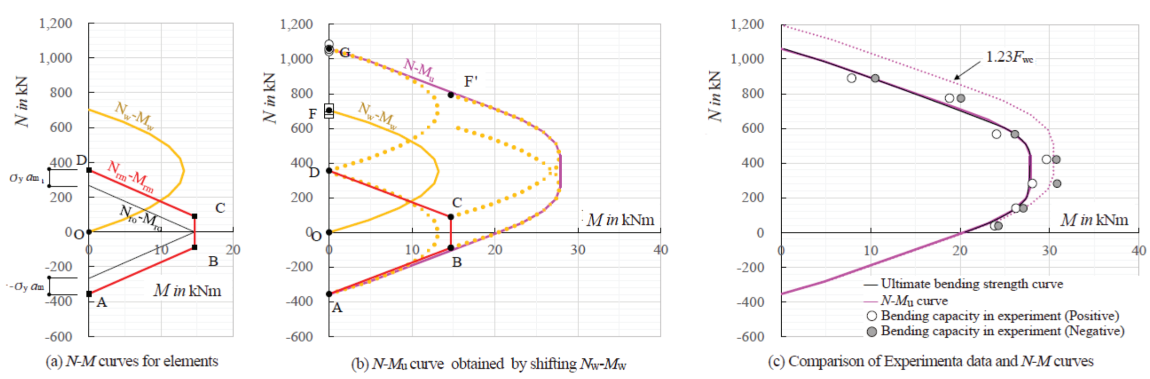


***Figure 13:** Comparison of N-M curves by using superposition method for estimating bending strength*



https://doi.org/10.52202/080513-0690

The $N_w$-$M_w$ relationship according to Equation (5) is shown in Figure 13(a) as a yellow solid curve. In the generalized superposed strength method concept, the envelope of the locus obtained by moving the point O at the origin of the yellow curve along the red polyline line in the figure from point A to point D can be used as the correlation curve ($N$-$M_u$ curve) for axial force-bending resistance when the rebar and timber are resisting as a single unit. Figure13(b) shows the yellow dotted curves for the case where point O of the yellow curve is placed at each of points A to D. The envelope of the locus is shown by connecting the pink curve and the straight line. When point O on the $N_w$-$M_w$ curve is moved from point C to point D, point F on the $N_w$-$M_w$ curve also moves linearly by the same vector as point C. The point F after the movement is called point F'. The locus of point F' is not the same as the envelope of the yellow dotted curve, so the envelope of the tangent lines of the slopes of points C and D is taken as the envelope of the yellow dotted curve with point O at point D. The same was done when moving point O between points A and B.

### 5.3 COMPARISION WITH EXPERIMENTS

In Figure 13(b), the experimental values for the specimens (WO, HW) subjected to compression loading are plotted by squares and circles, in which their moments are assumed to be zero. The squares indicate WO; the circles indicate HW. The experimental values for WO are estimated, with high accuracy, using the calculated values of the pink curve, which is the sum of the compressive yield strength of the timber and the rebars.

Figure 13(c) shows a comparison of the $N$-$M_u$ curve based on the generalized superposed strength method and the experimental values. The pink solid curve is the curve in Figure 13(b). The circles and triangles are the experimental values for bending strength, with the circles representing positive loading and the triangles representing negative loading. The $N$-$M_u$ curve calculated by the computer roughly estimates the experimental values for bending strength, but in the range of 200-800kN on the vertical axis, the experimental values are underestimated. In this range, the compressive strength of timber in the bending-compression range approaches the bending strength of timber. The bending strength of timber is greater than its compressive strength.

The calculation of the same curve uses the experimental values from the compression test, so it takes no account of the increase in the compressive strength of timber in the bending-compression range. The E65-F255 standard strength of the cedar timber used in this test has a ratio of 25.5 N/mm$^2$ for bending strength to 20.6 N/mm$^2$ for compressive strength, which is 1.23. The curve calculated multiplying this ratio by the compressive strength of timber (31.2 N/mm$^2$) is shown in pink dotted curves. The increase in the experimental value of bending capacity might also be due to the strain hardening effect of the rebars but based on the calculation of the bending ultimate strength described in the next section, the tensile strain of the tensile steel bars is around 1.5%, so the strain hardening effect is

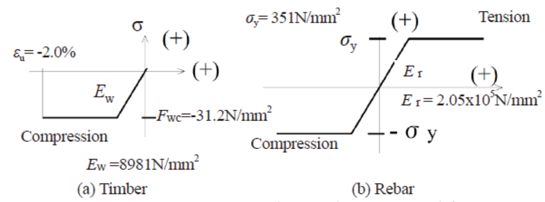


***Figure 14:*** *Stress-strain relationship assumed for ultimate bending strength of column*

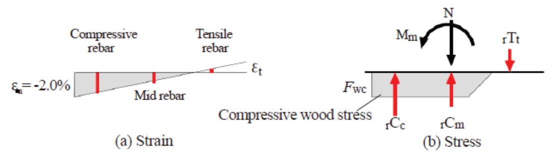


***Figure 15:*** *Profile of column's strain and stress by bending*

small. Therefore, the reason for the aforementioned underestimation of bending strength is probably due to on the increase of the compressive strength of the wood in the bending-compression.

### 5.4 CALCULARION FOR UTIMATE BENDING STRENGTH CAPACITY

The ultimate bending strength $M$u can be calculated using the compressive stress-strain relationship of wood in the bending-compression range, the stress-strain relationship of rebar, and the assumption of the plane section after bending.

Figure 14 shows the stress-strain relationship and the stress state of the cross-section for calculation. The ultimate bending capacity is defined as the bending moment at which the strain at the compression edge of the timber is equal to 2.0%, assuming that the limit strain for compression of timber is 2.0%. The $N$-$M$ curve based on this is shown in Figure 13(c) as a black solid curve. This black curve is almost identical to the $N$-$M_u$ pink curve by the generalized superposed strength method. This supports the fact that the bending strength of the composite column can be estimated using the simple superposed strength method.

### 5.5 EQUATIONS FOR BENDING STRENGTH

In Figure13(c), the $N$-$M$ curve based on the simple superposed strength method, the $N$-$M_u$ curve based on the generalized superposed strength method, and the $N$-$M_w$ curve based on calculations of the ultimate bending strength are almost identical. For the estimation of bending strength in designs where the lower limit is to be controlled, the compressive strength of timber in the bending-compression range is not the bending strength of timber but the compressive strength. In design, the standard values are used, so the estimation is even safer. The simple superposed strength equation for estimating bending strength is expressed as the followings. The axial force $N$ of the column is assumed to be positive for compression.

$$F_{wc}\, b\, D + a_m\, \sigma_y \leq N < N_{max}:$$

$$M_u = a_t\, \sigma_y\, j\, \{1 - (N - F_{wc}\, b\, D - a_m\, \sigma_y)/(2\, a_t\, \sigma_y)\} \tag{6.1}$$

$0.5F_{wc}bD + a_m\sigma_y \le N < F_{wc}bD + a_m\sigma_y$:

$$M_u = a_t\sigma_{yj} + 0.5(N - a_m\sigma_y)D\{1-(N - a_m\sigma_y)/(F_{wc}bD)\} \qquad (6.2)$$

$0.5F_{wc}bD - a_m\sigma_y \le N < 0.5F_{wc}bD + a_m\sigma_y)$:

$$M_u = a_t\sigma_y j + 0.125F_{wc}bD^2 \qquad (6.3)$$

$-a_m\sigma_y \leqq N < 0.5F_{wc}bD - a_m\sigma_y$ :

$$M_u = a_t\sigma_y j + 0.5(N + a_m\sigma_y)D\{1-(N + a_m\sigma_y)/(F_{wc}bD)\} \qquad (6.4)$$

$N_{min} \le N < -a_m\sigma_y$ :

$$M_u = a_t\sigma_y j\{1+(N + a_m\sigma_y)/(2a_t\sigma_y)\} \qquad (6.5)$$

Where, $N_{max}=F_{wc}bD+2a_t\sigma_y+a_m\sigma_y$, $N_{min}=-2a_t\sigma_y-a_m\sigma_y$

In general, the axial force ratio of the column under long-term load is 0.10-0.20 for $\eta$ with respect to the axial capacity of the composite column, and even when considering the variable axial force during a major earthquake, it is 0.20-0.40, so the axial force ratio with respect to the axial capacity of the composite column is approximately 0.40 or less, and in most cases, the bending strength capacity can be estimated using Equations (6.3) and (6.4).

## 6 − MOMENT-ROTATION RELATIONSHIP CALCULATED

### 6.1 CALCULATION

Calculation for the specimens was carried out assuming a history loop of the stress-strain relationship in which the timber and the rebar be subjected to repetitive stress. Figure 16 shows the spring model of the column. The upper part from the central height of the specimen in Figure 7 to the one-way pin above was modelled. Considering the thickness of the split steel plate, the section from the central height of the test section to the steel pipe (194 mm) was set as the elasto-plastic hinge section, and the section above was set as rigid.
A constant vertical load $V$ was applied to the top of the column, and positive and negative repeated moments were applied. The rotation angle of the hinge section was controlled so that the rotation angle history matched the experimental history. The additional moment of the central height column cross-section due to the vertical load $V$ was considered.

### 6. 2 MATERIAL PROPERTIES

The stress-strain relationship of timber and rebar was made to match Figure 14. As shown in Figure 17, the timber was made to be a trilinear stiffness-reducing type hysteresis model, and the rebar was made to be a modified Ramberg-Osgood type. The various values required for the settings are shown in the figure. Figure 18 shows an example of the stress-strain relationships of the timber and rebar springs at the hinge section, obtained from the calculation.

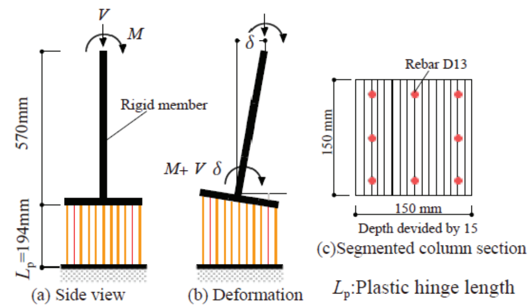


***Figure 16:*** *MS model and Segmented cross-section for column*

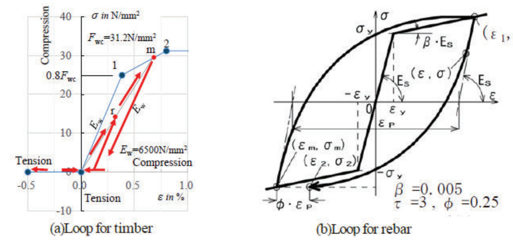


***Figure 17:*** *Assumed stress-strain curves under reversed*

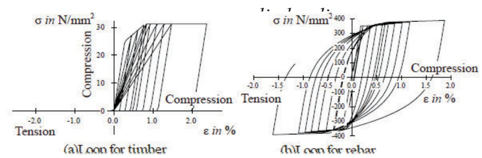


***Figure 18:*** *Stress-strain loops of springs in calculation for $\eta_w$=0.4*

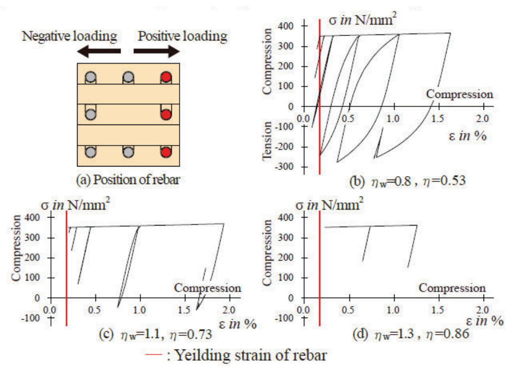


***Figure 19:*** *Moment-strain loops of a rebar in calculation for $\eta_w$=0.8-1.3*

### 6.3 MOMENT-ROTATION RELATIONSHIP

The moment-angle relationship ($M$-$\theta$ relationship) calculated is shown in Figure 11 as a pink curve. The calculated hysteresis loop is generally consistent with the experimental hysteresis loop, up to the point where a vertical crack appears in the column, ×, for specimens with $\eta_w$ of 0.05 and 0.2, up to the end of loading for specimens with $\eta_w$ of 0.4, and up to the maximum moment, ▲, for specimens with $\eta_w$ of 0.6 and 0.8. generally corresponded to the experimental history loop. The, ×, in the $M$-$\theta$ relationship is the point at which the strain in the timber at the bending edge of the column reached 2%. $\eta_w$ of 1.1 and 1.3 are approaching the perfectly elastic loop as described in Section 4.5


https://doi.org/10.52202/080513-0690

## 6.4 COMPARISION WITH RC COLUMN

As mentioned in Section 3.4, the moment-rotation angle relationship for one direction bending calculation of the specimens in which the wood has been replaced with concrete is shown in the positive and negative directions in Fig. 4. The stress-strain relationship for the concrete and rebar was assumed to be the same as in Section 3.4. The amount of rebar was of two types: one with a ratio of 2.49% ($p_g$), which was the same as the limit value for the rebar ratio of RC, and one with a ratio of 4.52% ($p_g$), which was the same as the HW specimen.

The former is shown as RC249 with light blue dotted curve, and the latter is shown as RC452 with light blue solid curve.

Regarding initial bending stiffness, in the range where $\eta_w$ is small (0.05-0.4) and the axial force is small, the bending tensile range of wood and concrete does not resist tension, so the bending stiffness of the composite column is not as large as the difference in compressive stiffness in Section 3.4, and is about the same as that of RC249, which has a smaller amount of rebar due to the limit on the rebar ratio.

As the axial force increases, the bending and tensile range of the column cross-section decreases, and the effect of the compressive stiffness of the concrete becomes greater, so the bending stiffness of the RC column becomes greater. The bending stiffness of RC452 is greater than that of the composite timber column.

In the case of $\eta_w$ = 0.05 and 0.2, where the axial force is small, the concrete compresses and breaks, but the rebar alone is able to support the axial force and moment, and a certain level of resistance is maintained. However, when $\eta_w$ is 0.4 or more, the axial resistance is insufficient, and the bending moment capacity also decreases rapidly. This indicates axial collapse. In the calculation, the buckling of the rebar in the column due to the compression crush of the concrete is not taken into account, so in reality the decrease will be more rapid. After the concrete in the RC column reaches its compressive strength, the rebars will buckle prematurely due to repeated loading if they are not restrained by the large number of stirrups, so the ductility of the RC column will decrease considerably. As mentioned above, in general design, the axial force of the column is limited to 0.3-0.6 for $\eta_w$ , i.e. 0.2-0.4 for $\eta$, in the case of a major earthquake, so this suggests that, within this range, the bending stiffness, bending capacity and toughness of the composite timber column are extremely superior to those of the RC column.

Furthermore, because the weight of the structural members of the composite timber building is reduced to 1/3 compared to that of the RC building, the composite timber building probably exhibits extremely superior seismic performance.

## 7－ SUMMARY

With the aim of clarifying the correlation between axial force and bending capacity of the yielding hinge of column connected to the reinforced concrete foundation, and the method of estimating that, compression test and repetitive bending loading test were conducted on the yielding hinge of columns. The followings were clarified.

1) The composite timber column subjected to uniaxial compression force has increased compressive stiffness, compressive strength, and toughness due to the rebar. The limit compressive strain at which compressive strength can be maintained can be expected to be up to 2.0%, and the limit strain is determined by the buckling of the rebar. Compared to reinforced concrete columns where timber is replaced with concrete, the initial compressive stiffness is somewhat smaller, but the compressive strength was 1.23 times greater, and the limit compressive strain is approximately 7.0 times greater, demonstrating extremely high ductility.
2) If the axial force ratio $\eta$ is 0.4 or less, the composite timber column demonstrates stable bending capacity even when subjected to bending force, up to a large deformation angle of $3.0x10^{-2}$rad. and almost no damage occurs to the timber up to $2.0x10^{-2}$ rad.
3) The compressive deformation toughness of the composite timber columns is extremely high, so the bending strength can be accurately estimated using the simple superposed strength method based on plasticity, and the correlation curve between axial force and bending strength and the bending strength estimation equation are shown.
4) When subjected to axial force and bending, calculations show that when the axial force ratio $\eta$ is 0.53 or less, the bending stiffness of the composite timber column is similar to that of a reinforced concrete column, which has a limit on the rebar ratio, and it also demonstrates extremely excellent performance in terms of bending capacity and ductility.

## 8-ACKNOWLEDGEMENT

This project was funded as Grants-in-Aid for Scientific Research 'A' by Japan Society for the Promotion of Science, 2023.

## 9－REFFERENCE

[1] S.Shioya, et al. : An innovative hybrid timber structure in Japan: performance of column and beam, WCTE 2016
[2] M. Mukai, et al. : Horizontal - loading test of steel bar - timber composite column for mid-rise building, WCTE 2021
[3] Y. Shimoirisa, et al. : Horizontal-loading test of steel bar-timber composite columns for low-rise building, Oslo, WCTE2023
[4] K. Hayata, et al.: Experiement on axial capacity-bending capacity relationship of steel rebar-timber composite column, Oslo, WCTE2023